(INVITED)Dispersion-shifted tellurite fibers for nonlinear frequency conversion

M. Evrard, E. Serrano, C. Strutynski, F. Désévédavy, G. Gadret, J.C. Jules, B. Kibler, F. Smektala

Optical Materials: X 15 (2022) 100183

Contents lists available at ScienceDirect

Optical Materials: X

journal homepage: www.journals.elsevier.com/optical-materials-x

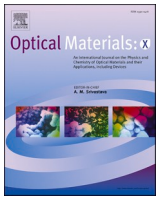

Invited Article

(INVITED)Dispersion-shifted tellurite fibers for nonlinear frequency conversion

M. Evrard [1], E. Serrano [1], C. Strutynski, F. Désévédavy, G. Gadret, J.C. Jules, B. Kibler [*], F. Smektala

Laboratoire Interdisciplinaire Carnot de Bourgogne, UMR6303 CNRS-Université Bourgogne Franche-Comté, 9 Avenue Alain Savary, 21078, Dijon Cedex, France

ARTICLE INFO

Keywords:
Tellurite glasses
Dispersion-shifted fibers
Mid-infrared
Frequency conversion
Refractive index measurement

ABSTRACT

We report a detailed numerical investigation of step-index tellurite fiber properties based on the careful experimental characterization of refractive indices for two tellurite-glass systems employed in fiber manufacturing. More specifically, our study focuses on two typical step-index configurations, namely weak and strong index differences between core and cladding glasses. We reveal that a wide range of dispersion-shifted features for tellurite fibers can be obtained in the 2–3 μm range combined with small or large effective mode areas. Our work also outlines the potential application of such dispersion-engineered fibers for nonlinear wavelength converters between near- and mid-infrared regions.

1. Introduction

Single-mode dispersion-shifted fibers (DSFs) have been first developed in the 80's based on silica glasses [1,2] to offer significant benefits for long-haul telecommunication systems. The main objective was to shift the zero-dispersion wavelength from 1.3 μm to the 1.55-μm wavelength range, and take advantage of inherent lower attenuation as well. By contrast to standard single-mode step-index fibers, a particular design of refractive index profile is required with a higher dopant level into the core, thus implying a reduced mode-field diameter. Later on, another generation of DSFs has been developed with engineered dispersion for parametric and Raman amplification schemes [3–6]. All-optical wavelength amplification or conversion based on four-wave mixing in a fiber has then emerged as an attractive solution owing to the quasi-instantaneous response of the Kerr nonlinearity of fused silica. To widen the range of optical amplifiers, one needs for dispersion designs covering a wide range of wavelengths around 1.5 μm. The main challenge to manage higher-order dispersions of DSFs mainly relies on achieving complex index profiles based on multi-layered structures. Next, newly developed dispersion-shifted highly-nonlinear fibers have enhanced properties of such fiber-optic parametric amplifiers and wavelength converters [7–10], in particular by achieving relatively large conversion efficiency with short fiber lengths.

Typically, phase-matching for efficient parametric gain requires pumping in the low anomalous dispersion regime, however a low normal dispersion regime pump can provide far-detuned phase-matched frequencies through a suitable group-velocity dispersion profile [11,12]. Nowadays, fiber-optic parametric amplifiers/converters still rely on conventional silica fibers (albeit tailored through a suitable combination of GeO_2-doping of the core, a reduced core diameter, and a W-shaped refractive index profile) when operating around the 1.55 μm window [13]. The use of microstructured or tapered optical fibers has been the subject of much recent work [14–17], since it allows extending the range of attainable wavelengths down to the 1-μm range and below with silica glass, or beyond 2 μm with chalcogenide-based glasses. The transition between the near-infrared and mid-infrared region (i.e., 1.5–3.5 μm band) remains a challenging issue for developing efficient fiber platforms for parametric conversion. Only soft glasses such as fluorides and tellurites exhibit suitable bulk dispersion and transmission losses in this spectral range [18], thus allowing the simple use of conventional step-index profiles for DSF manufacturing. However, when dealing with nonlinear devices, tellurite glasses appear as a more relevant alternative due to their transparent window from visible up to ~6.5 μm and their higher nonlinear properties [19].

Several nonlinear applications of tellurite fibers have already been reported in literature such as supercontinuum light sources [20–22], Raman and Brillouin lasers [23–25], and frequency combs [26]. It is worth to mention that wavelength conversion based on the four-wave

* Corresponding author.
E-mail address: bertrand.kibler@u-bourgogne.fr (B. Kibler).
[1] These authors contributed equally to this work.

https://doi.org/10.1016/j.omx.2022.100183
Received 18 July 2022; Received in revised form 25 August 2022; Accepted 25 August 2022
Available online 7 September 2022

mixing process has been investigated in a tellurite step-index fiber as short as 1 m [27]. However, the conversion bandwidth remains here limited to the 1.4–2.4 μm band, the pumping operated around 1.8 μm near the zero-dispersion wavelength of the fundamental mode. A fine control of zero-dispersion wavelength (ZDW) as well as dispersion profile is then crucial to manage the phase-matching condition over a larger bandwidth as a function of the laser pumping and the signal band to convert. When dealing with step-index fibers and tellurite glasses whose bulk ZDW is usually between 2 and 2.5 μm [28], most of studies have reported on the development of fibers which exhibit a ZDW below 2 μm, even by using a more complex W-type index profile or double-clad scheme [29,30]. Only recently, we have demonstrated that the location of ZDW can be easily modulated by modifying the core diameter of a simple step-index tellurite fiber [31,32]. However, in general, the full dispersion profile over the transparency window of the fiber is not known with a sufficiently good precision to meet the requirements for developing accurate wavelength converters/amplifiers beyond 2 μm.

In this work, we report on the numerical analysis of dispersion-shifted step-index tellurite fibers based on the accurate refractive index measurements of purified TeO_2–ZnO–Na_2O (TZN) and TeO_2–ZnO–La_2O_3 (TZL) glasses. Index measurements are here performed by ellipsometry on the 0.5–4.0 μm range on bulk samples of core and cladding glass compositions, and full dispersion curves of the fundamental mode of corresponding fibers are calculated. In particular, we show that position of the shifted ZDW can be finely controlled over the 2.0–2.5 μm range. Two distinct index profiles are studied, namely a low ($\sim 1.2 \times 10^{-2}$) and high refractive index difference ($\sim 1.2 \times 10^{-1}$) in the spectral range under study. Such results open new perspectives for step-index tellurite fibers as promising solutions for the next generation of linear/nonlinear photonic devices in the spectral region covering the transition between near- and mid-IR, combined with recent lasers sources based on thulium/holmium-doped fibers. To this end, we finally investigate the spontaneous parametric gain induced by fourth-order dispersion in tellurite fibers as possible future far-detuned wavelength converters towards the 4-μm band.

2. Experimental characterization of tellurite glasses

2.1. Glass synthesis and fiber manufacturing

We have recently reported on the TZL and TZN glasses manufacturing and purification process: for more details, the reader can refer to Refs. [33–36]. Preforms syntheses are made from the classical melt-quenching method. All the fabrication process is realized under controlled atmosphere (dry air) where H_2O concentration is monitored to keep the value under 0.5 ppm (vol.), which allows for OH contamination from powders and atmosphere to be reduced, more specifically raw materials storage and weighing in platinum crucibles, synthesis (in an electric furnace under pure O_2), quenching and annealing. Compositions of the core/cladding combinations of glasses are respectively $70TeO_2$–25ZnO-$4.25La_2O_3$-$0.75La_2F_6$ (TZLF)/$65TeO_2$–30ZnO–$5La_2O_3$ (TZL) and $80TeO_2$–5ZnO–$10Na_2O$–$5ZnF_2$ (TZNF)/$60TeO_2$–$20Na_2O$-$15GeO_2$-5ZnO (TNaGZ). High purity oxide (TeO_2, ZnO, Na_2O, La_2O_3: Fox Chemicals 99.999%) and fluoride (LaF_3, Alfa Aesar 99.99%, here introduced as La_2F_6) precursors are also employed also to limit OH-groupments into the vitreous matrix. Fluorine introduction in the core composition ensures to significantly reduce the OH contamination in the mid-infrared (mid-IR). Step-index fibers are manufactured by combining the Built-in-Casting (BiC) process to the Rod-in-Tube (RiT) one: as previously described in other works, a large core step-index preform is prepared by BiC process [33] and core-cladding canes are then obtained by thermal elongation and introduced into a drilled preform by RiT process. Small-core step-index fibers can then be drawn from this preform. Internal and external claddings for each fiber are made from the same compositions: respectively TZL for the first fiber and TNaGZ for the second one. Fiber drawing is possible by using a 3-m tower with an annular furnace in which the temperature is increased to reach the softening regime. Parameters can be tuned during drawing, such as speeds of preform descent into the furnace or cylinder rotation, to modify fiber diameter and then the core size.

2.2. Transmission spectrum and index measurements

Transmission spectra of core glasses are recorded, in the present work, in the UV–Visible and near-IR regions with a Perkin-Elmer Lambda 900 spectrometer, and with a Fourier transform infrared Perkin-Elmer spectrometer (Spectrum One) for the mid-IR range (see Fig. 1a). For both core compositions, transmission spectra are comparable. Thanks to purification process, unwanted absorptions between 3 and 5 μm due to OH groups are drastically reduced. For the two compositions, the bandgap is observed at 0.37 μm and multiphonon absorption cut-off is at 6.20 μm for TZLF and 6.17 μm for TZNF. We note that transmission rate on the 0.5–4.5 μm spectral range is of 78% for both glasses. The 22% remaining are due to the Fresnel losses at the sample interfaces (11% for each interface).

The linear refractive index evolution of core and cladding compositions as a function of the wavelength is measured by using a Variable Angle Spectroscopic Ellipsometer (VASE) from J. A. WOOLLAM with standard configuration of rotating polarizer. A Xenon light source is used for emission, and then guided to the monochromator (HS-190 model) by a ZrF_4 optical fiber. Measurements are then performed on the 0.5–4.0 μm range, in the transmission range of the ZrF_4 fiber, by keeping a constant incidence angle. Two detectors are employed in order to performed measurements on the full spectral range from visible to 4 μm. A first standard detector stacked from two detection elements is used up to 2.5 μm. Measurements in the visible and up to 1 μm range are performed by using a silicon detector, and combined with an extended InGaS detector for the 1.0–2.5 μm range. Beyond 2.5 μm, an InSb detector is then employed. Calibration of the ellipsometer has been carefully performed on standard samples such as fused silica for which measurements have been intensively collected since 1965 [37]. However, contrary to transmission measurements which require samples with two parallel and “mirror-polished” faces, refractive index measurements by ellipsometry require only one “mirror-polished” face but with higher quality of polishing. Polishing is first realized with silicon carbide (SiC) wheels by decreasing size grading to 4000 (5 μm-diameter grains). Then, an abrasive diamond polishing paste, with diamond particles diameters decreasing from 3 to 0.1 μm, is employed on a felt wheel, to enhance the surface quality of glass samples. After measurements, the full wavelength-dependent refractive index curves for each core/cladding combinations are determined from fitting data obtained from ellipsometry with a two-pole Sellmeier equation (1) [28,38]:

$$n^2(\lambda) = A + \frac{B\lambda^2}{\lambda^2 - C^2} + \frac{D\lambda^2}{\lambda^2 - E^2} \quad (1)$$

with λ the wavelength and A, B, C, D and E the Sellmeier coefficients obtained specifically for each glass composition. Sellmeier fits for both glass compositions are plotted together with experimental measurements in Fig. 1. Sellmeier coefficients of the equation are gathered in Table 1 for the four glass compositions.

The difference between core and cladding indices does not exceed 1.5×10^{-2} for the TZLF/TZL combination (Fig. 1b), it remains quasi-constant between 2 and 3 μm with a refractive index difference of 1.2×10^{-2}, and a calculated numerical aperture (NA) about 0.22. However, the index difference is nearly 10 times higher for the TZNF/TNaGZ combination (Fig. 1c) for which the gap is about 1.2×10^{-1}, especially between 2 and 3 μm. The numerical aperture for this glass combination is 0.67. As expected, the numerical aperture for the TZN-glass fiber system is larger, about 3 times the NA of TZL-glass combination.

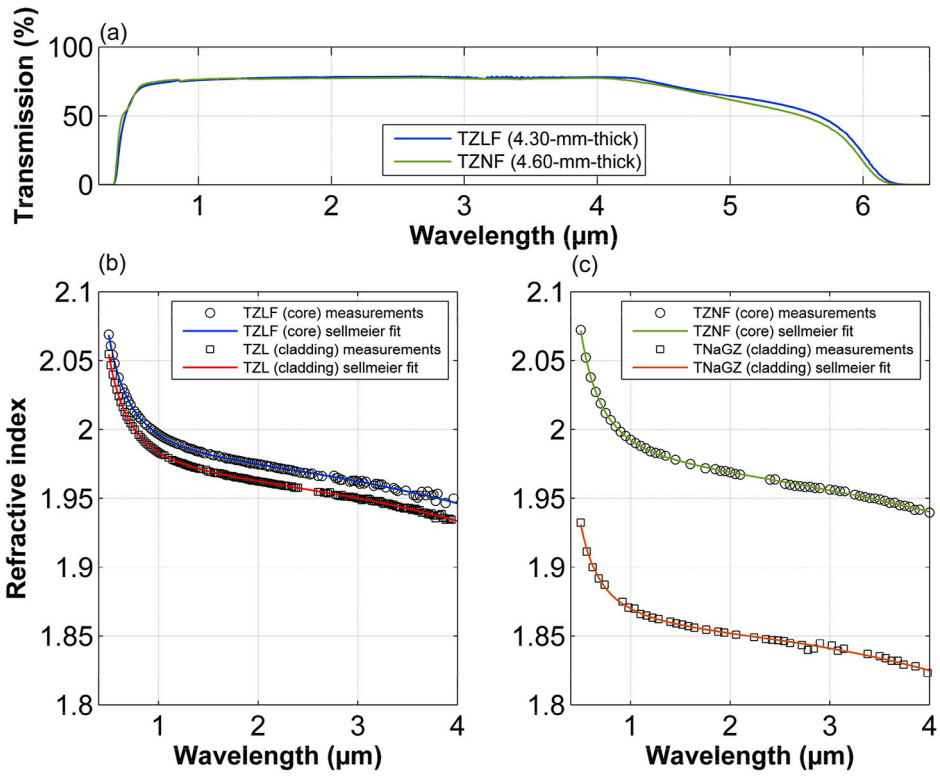

Fig. 1. - (a) Transmission spectra of our tellurite core compositions. (b,c) Wavelength-dependent refractive indices with Sellmeier fits for TZLF/TZL and TZNF/TNaGZ compositions, respectively.

Table 1
Sellmeier coefficients obtained by a least-square fitting procedure for tellurite core and cladding compositions.

Role	Glass sample	A	B	C (μm)	D	E (μm)
CORE	TZLF	0.67321	3.23196	0.16139	0.63972	9.97791
CLADDING	TZL	1.60069	2.25886	0.18598	0.6976	10.22841
CORE	TZNF	0.94476	2.93952	0.175	2.36655	17.82988
CLADDING	TNaGZ	1.84459	1.5929	0.1971	0.38494	8.46607

3. Numerical study of fiber properties

3.1. Properties of the fundamental mode

The wavelength-dependent refractive index curve obtained for each tellurite glass allows now to calculate the normalized frequency V for a step-index profile with varying core radius through the relation (2), where ϕ_{core} is the core diameter, λ is the propagating light wavelength and n_{core} and n_{clad} the core and cladding refractive indices, respectively.

$$V = \frac{\pi \phi_{core}}{\lambda} \sqrt{n_{core}^2 - n_{clad}^2} \quad (2)$$

Corresponding calculations for step-index fibers using both TZL- and TZN-glass systems are shown in Fig. 2. For TZL fibers, we observe that a core diameter around 7 μm is requested to exhibit a single-mode behavior beyond the 2-μm wavelength band. This core size then appears as an interesting solution for matching standard silica fibers dedicated to single-mode 2-μm laser delivery (e.g., SM1950 and SM2000 fibers). By contrast, our TZN-glass fibers show that a single-mode behavior in the same spectral range would be only possible for a core diameter about 3 μm. Nevertheless, we have already demonstrated that larger fiber cores (i.e., few-mode fibers) can be used for nonlinear applications with both easy and efficient coupling into the fundamental mode [22]. Moreover, such tellurite fibers with small cores would be compatible to ultra-high NA silica fibers with high GeO_2-doping content

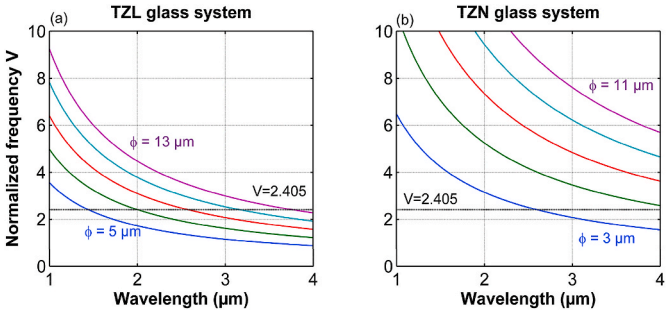

Fig. 2. Calculated normalized frequency parameter V for our step-index tellurite fibers with (a) core diameters ϕ_{core} = 5, 7, 9, 11 and 13 μm in the TZL-glass system and (b) core diameters ϕ_{core} = 3, 5, 7, 9 and 11 μm in the TZN-glass system. Dashed black line indicates the single-mode behavior limit (V = 2.405).

[25].

Next, based on this simple step-index profile, we evaluated dispersion curves for the fundamental mode HE_{11} for all core diameters and glass compositions by numerically solving the dispersion equation (also called the eigenvalue equation) for cylindrical step-index waveguides. The dispersion curves presented are therefore based on the above index measurements carried out on the bulk materials. Fig. 3a-**3**b report the

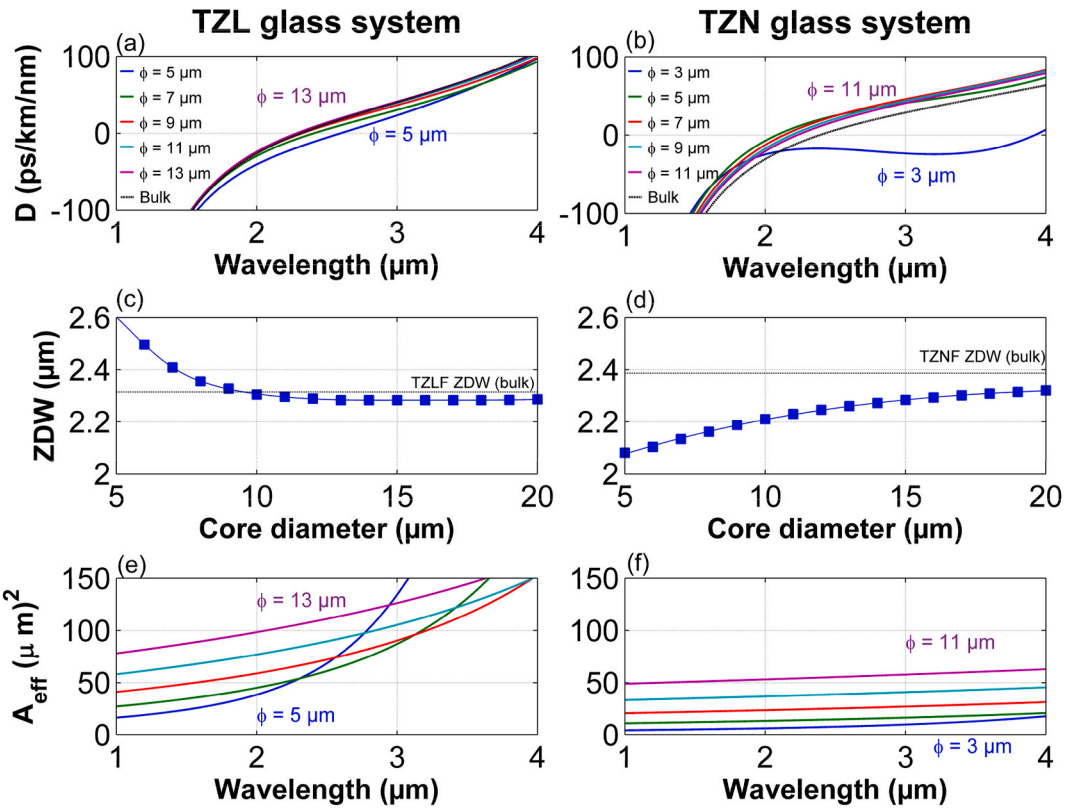

Fig. 3. Numerically calculated wavelength-dependent curves of dispersion of the fundamental guided mode for step-index fibers (a) in the TZL-glass system with ϕ_{core} = 5,7,9,11 and 13 μm, and (b) in the TZN-glass system with ϕ_{core} = 3,5,7,9 and 11 μm. (c–d) Evolution of the zero-dispersion wavelength as a function of core diameter for TZL and TZN fibers, respectively. (e–f) Calculated effective mode area A_{eff} of the fundamental guided mode for step-index fibers in the TZL- and TZN-glass systems, respectively. Studied core diameters are the same as in subplots (a) and (b).

calculated dispersion curves for both TZL- and TZN-glass systems. We find that a normal dispersion regime is always found in both glass systems for wavelengths below 2 μm, while the anomalous dispersion is obtained beyond 3 μm as soon as core diameters are larger than ~5 μm. Main differences occur in the spectral range (2–3 μm) around the bulk's ZDW of core glasses (here located about 2.3–2.4 μm). Fig. 3c-**3**d clearly show distinct behaviors of the evolution of the ZDW as a function of fiber core size for the two glass systems. For a small core/clad index difference (TZL-glass system), the ZDW is shifted toward longer wavelengths with decreasing core diameters. The zero-dispersion position can be easily varied from 2.3 to 2.6 μm. This change is similar to that occurs in single-mode silica fibers with DSF development to shift the ZDW from 1.3 to 1.55 μm. On the contrary, for our TZN-glass system, the ZDW is shifted toward lower wavelengths for decreasing core diameters, typically from 2.3 to below 2.1 μm. With two simple glass combinations, we are able to control the shift of ZDW over a large spectral band of interest from 2 to 2.6 μm.

The wavelength-dependent curves of effective mode field areas A_{eff} are also calculated and shown in Fig. 3e-**3**f. By comparing the two glass systems, one notices that for a given wavelength, the effective area is much smaller for TZN step-index fibers than for TZL fibers, this simply relies on the large core/clad index difference. For example, at 2-μm wavelength and 5-μm core diameter, the effective area for a TZL fiber is nearly three times larger than for a TZN fiber. The corresponding nonlinear coefficient ($\gamma = 2\pi n_2/\lambda A_{eff}$, with n_2 the nonlinear index) of step-index fibers thus appears to be significantly higher for our TZN composition than for TZL-glass system. As a consequence, our TZN fibers with a large index difference are clearly suitable for nonlinear applications, as already highlighted in Refs. [31–33], while our TZL fibers could be applied for linear devices. In the particular case of TZL fibers with small index difference, we also observe that the field distribution extends significantly beyond the core for wavelengths above 3 μm and core size below 7 μm, thus leading to very large effective areas (see Fig. 3e). Here, such single-mode fibers will become increasingly sensitive to bend losses and small imperfections at long wavelengths, with typical high confinement losses.

3.2. Application to dispersion compensation

Standard single-mode silica and fluoride fibers exhibit anomalous dispersion ($D > 0$) in the 2-μm wavelength band and beyond [39]. Then, small-core germano-silicate fibers have been used for dispersion compensation in the 2-μm wavelength range, for instance with application to fiber laser/amplifier systems covering thulium and holmium emission [40]. Here we propose our TZL-glass combination with small index difference as an interesting alternative. A detailed analysis of dispersion in the 1.8–2.3 μm window (see Fig. 4) shows that large dispersion tailoring over negative values can be enabled through a simple variation of the core size. Such fibers will exhibit similar nonlinear coefficients to small-core silica-based fibers, since the larger A_{eff} being compensated by the higher n_2 in TZL fibers [19]. We also underline that it is generally not sufficient to compensate the second-order dispersion only. Future designs of tellurite fibers for dispersion compensation should also deal with higher-order dispersion, while keeping the mode-matching as a crucial issue.

3.3. Application to nonlinear frequency converters

The strong optical confinement and varying dispersive properties for our TZN step-index fibers with large index difference have already enabled interesting nonlinear applications around 2 μm such as Brillouin lasing and ultrabroadband supercontinuum generation in very short

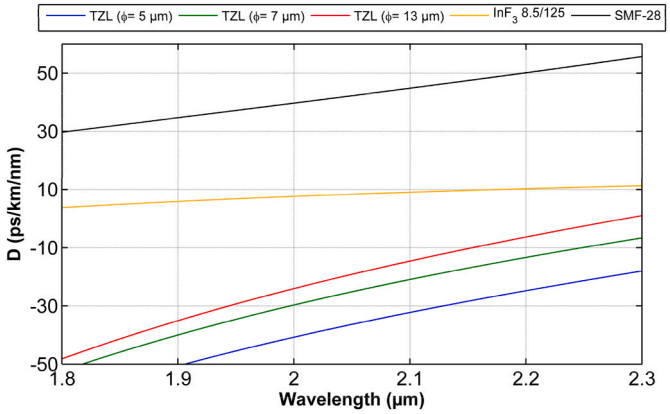

Fig. 4. – Dispersion curves of TZL step-index fibers with varying core diameters in the 1.8–2.3 μm window. We provide the comparison with dispersion curves of commercially-available standard single-mode silica (SMF-28) and fluoride (InF_3) fibers [39].

fiber lengths [22,25], and demonstrating the possible guiding of wavelengths beyond 4.5 μm. Here we investigate the potential of our TZN fibers as future band converters from near-infrared to the mid-infrared region towards the 4-μm band, through the spontaneous modulation instability (MI) process induced by fourth-order dispersion mainly. In the frequency domain, this leads to the emergence of two far-detuned frequency sidebands placed symmetrically with respect to the pump frequency. In order to get these two sidebands emerging far from the pump, the group-velocity dispersion β_2 has to be positive (normal dispersion regime) and the fourth-order dispersion term β_4 negative [12]. This phenomenon has been studied for several types of fibers by pumping in the normal dispersion regime close to the ZDW. The derivation of the phase-matching condition should include higher-order terms of the Taylor expansion of the propagation constant $\beta(\omega)$ when β_2 is relatively small. Only the even-order terms contribute to the phase-mismatch, so that the full phase-matching relation takes the following form [11]:

$$\sum_{m=2,4,\ldots}^{\infty} \frac{\beta_m \Omega^m}{m!} + \gamma P = 0 \tag{3}$$

with Ω the frequency shift of the symmetric Stokes and anti-Stokes sidebands from the pump, β_m are the dispersion coefficients calculated at pump frequency, and P the initial peak power. The nonlinear Kerr coefficient γ is calculated from the effective mode area and the nonlinear refractive index $n_2 = 3.8.10^{-19}$ m^2 W^{-1} [19].

As an example, this nonlinear process has been recently used for converting two mutually coherent frequency combs generated with electro-optic modulators at 1.55 μm in the 2-μm band [41]. This band converter is designed on fourth-order dispersion-induced modulation instability taking place in the normal dispersion regime of a highly nonlinear silica fiber and by seeding this phenomenon with a frequency agile and low-power laser around 1.3 μm. As a result, researchers have developed a stable and wavelength tunable all-fibered dual-comb spectrometer operating in the 2-μm region to investigate CO_2 absorption spectra. By means of intrinsic features of TZN fibers, we here propose to evaluate the possible frequency conversion well-above the 2-μm band, towards 4.2 μm, where molecular absorption is again significantly stronger and very short absorption path-length would be sufficient enough. To this end, we consider a pumping wavelength around 2 μm to convert a signal in the telecom bands close to 4.2 μm. For an accurate description of fiber dispersion curve over a broad spectral range, Taylor coefficients up to β_{10} are considered in relation (3). Fig. 5 presents the calculated phase-matching diagram of MI sidebands as a function of pumping wavelength for a 5-μm core TZN-glass fiber. Closely spaced

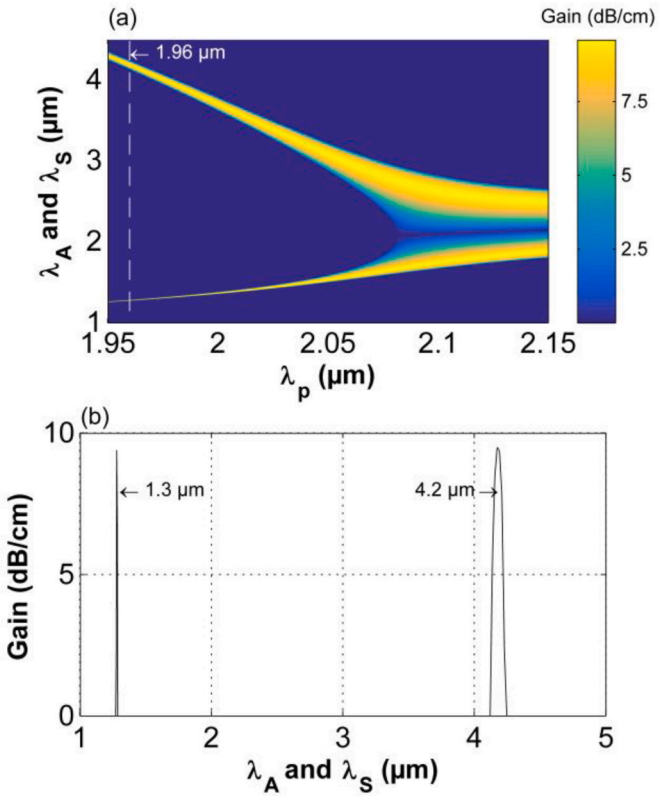

Fig. 5. – (a) False-color map of MI phase-matching diagram for a TZN step-index fiber with 5-μm core diameter. Color scale indicates corresponding spectral power gain in dB/cm. (b) Gain profile selected at the pumping wavelength (i.e., at 1.96 μm) that allows wavelength conversion around 4.2 μm. (For interpretation of the references to color in this figure legend, the reader is referred to the Web version of this article.)

sidebands are observed for pumping beyond 2.08 μm in the anomalous dispersion regime, this configuration corresponds to common MI gain induced by the second-order dispersion only. By contrast, when pumping in the normal dispersion regime (below 2.08 μm), we clearly note far-detuned sidebands with the typical narrow-band feature [12]. When pumping close to 1.96 μm with practical thulium-doped fiber lasers with a peak power of 1 kW, we report the potential use of our fiber as band converter from 1.3 to 4.2 μm, namely a 160-THz frequency shift, with significant efficiency (spontaneous gain almost reaches here 10 dB/cm). This confirms that short tellurite step-index fibers (only a few centimeters in length) are clearly suitable candidates for frequency converters between near-IR and mid-IR.

4. Conclusion

In this work, we have investigated the possible dispersion management in step-index tellurite fibers, in particular in the 2-μm waveband. This has been enabled by experimental characterization of refractive indices for two tellurite-glass systems recently employed in fiber manufacturing. Then, we have carried out a detailed numerical analysis of fiber properties based on two glass combinations which respectively exhibit a small and a high refractive index difference. Distinct features of dispersion-shifted fibers have been revealed, thus opening the way to future development of linear and nonlinear fiber devices. Finally, we have paid attention to the potential of short lengths of tellurite fibers as nonlinear frequency converters in the crucial spectral transition between near- and mid-infrared. We expect that our work propels further researches on the applications of tellurite fibers.

CRediT authorship contribution statement

M. Evrard: Formal analysis, Writing – original draft, Investigation, Visualization. **E. Serrano:** Writing – original draft, Writing – review & editing, Investigation, Software. **C. Strutynski:** Investigation. **F. Désévédavy:** Investigation. **G. Gadret:** Investigation, Methodology. **J. C. Jules:** Investigation. **B. Kibler:** Writing – original draft, Writing – review & editing, Conceptualization, Supervision, Visualization. **F. Smektala:** Project administration, Funding acquisition, Supervision.

Declaration of competing interest

The authors declare that they have no known competing financial interests or personal relationships that could have appeared to influence the work reported in this paper.

Acknowledgements

This work was supported by the Agence Nationale de la Recherche (TRAFIC project, contract no: ANR-18-CE08-0016; EQUIPEX + SMARTLIGHT platform, contract no: ANR-21-ESRE-0040; EIPHI Graduate School, contract no: ANR-17-EURE-0002) and by Bourgogne Franche-Comté region together with European Regional Development Fund. The authors thank K. Hammani and G. Millot for fruitful discussions.

References

[1] H. Shang, T.A. Lenahan, P.F. Glodis, D. Kalish, Dispersion-shifted depressed-clad triangular-profile single-mode fiber, in: Optical Fiber Communication, 1985 OSA Technical Digest Series, Optica Publishing Group, 1985 paper WD1.
[2] T.D. Croft, J.E. Ritter, V.A. Bhagavatula, Low-loss dispersion-shifted single-mode fiber manufactured by the OVD process, in: Optical Fiber Communication, 1985 OSA Technical Digest Series, Optica Publishing Group, 1985 paper WD2.
[3] K. Inoue, H. Toba, Wavelength conversion experiment using fiber four-wave mixing, IEEE Photon. Technol. Lett. 4 (1992) 69–72.
[4] F.S. Yang, M.E. Marhic, L.G. Kazovsky, CW fiber optical parametric amplifier with net gain and wavelength conversion efficiency >1, Electron. Lett. 32 (1996) 2336–2338.
[5] F. Koch, S.V. Chernikov, S.A.E. Lewis, J.R. Taylor, Characterisation of single stage, dual-pumped Raman fibre amplifiers for different gain fibre lengths, Electron. Lett. 36 (2000) 347–348.
[6] C.J.S. de Matos, D.A. Chestnut, P.C. Reeves-Hall, J.R. Taylor, 'Continuous-wave-pumped Raman-assisted fiber optical parametric amplifier and wavelength converter in conventional dispersion-shifted fiber, Opt Lett. 26 (2001) 1583–1585.
[7] G.A. Nowak, Y.-H. Kao, T.J. Xia, M.N. Islam, 'Low-power high-efficiency wavelength conversion based on modulational instability in high-nonlinearity fiber, Opt Lett. 23 (1998) 936–938.
[8] O. Aso, Shin-ichi Arai, T. Yagi, M. Tadakuma, Y. Suzuki, S. Namiki, 'Broadband four-wave mixing generation in short optical fibres, Electron. Lett. 36 (2000) 709–711.
[9] W. Imajuku, A. Takada, Y. Yamabayashi, 'Inline coherent optical amplifier with noise figure lower than 3dB quantum limit, Electron. Lett. 36 (2000) 63–64.
[10] J. Hansryd, P.A. Andrekson, 'Broad-band continuous-wave-pumped fiber optical parametric amplifier with 49-dB gain and wavelength-conversion efficiency, IEEE Photon. Technol. Lett. 13 (2001) 194–196.
[11] G.P. Agrawal, Nonlinear Fiber Optics, *sixth ed.*, Academic Press, London, 2019.
[12] S. Pitois, G. Millot, Experimental observation of a new modulational instability spectral window induced by fourth-order dispersion in a normally dispersive single-mode optical fiber, Opt Commun. 226 (2003) 415–422.
[13] P.A. Andrekson, M. Karlsson, Fiber-based phase-sensitive optical amplifiers and their applications, Adv. Opt Photon 12 (2020) 367–428.
[14] A. Chen, G. Wong, S. Murdoch, R. Leonhardt, J. Harvey, J. Knight, W. Wadsworth, P. Russell, Widely tunable optical parametric generation in a photonic crystal fiber, Opt. Lett. 30 (2005) 762–764.
[15] M.W. Lee, T. Sylvestre, M. Delqué, A. Kudlinski, A. Mussot, J.-F. Gleyze, A. Jolly, H. Maillotte, Demonstration of an all-fiber broadband optical parametric amplifier at 1 μm, IEEE J. Lightwave Technol. 28 (2010) 2173–2178.
[16] T. Godin, Y. Combes, R. Ahmad, M. Rochette, T. Sylvestre, J.M. Dudley, Far-detuned mid-infrared frequency conversion via normal dispersion modulation instability in chalcogenide microwires, Opt. Lett. 39 (2014) 1885–1888.
[17] S. Xing, D. Grassani, S. Kharitonov, L. Brilland, C. Caillaud, J. Trolès, C.-S. Brès, Mid-infrared continuous-wave parametric amplification in chalcogenide microstructured fibers, Optica 4 (2017) 643–648.
[18] G. Tao, H. Ebendorff-Heidepriem, A.M. Stolyarov, S. Danto, J.V. Badding, Y. Fink, J. Ballato, A.F. Abouraddy, Infrared fibers, Adv. Opt Photon 7 (2015) 379–458.
[19] M. Deroh, J.-C. Beugnot, K. Hammani, C. Finot, J. Fatome, F. Smektala, H. Maillotte, T. Sylvestre, B. Kibler, Comparative analysis of stimulated Brillouin scattering at 2 μm in various infrared glass-based optical fibers, J. Opt. Soc. Am. B 37 (2020) 3792–3800.
[20] P. Domachuk, N.A. Wolchover, M. Cronin-Golomb, A. Wang, A.K. George, C.M. B. Cordeiro, J.C. Knight, F.G. Omenetto, Over 4000 nm bandwidth of mid-IR supercontinuum generation in sub-centimeter segments of highly nonlinear tellurite PCFs, Opt Express 16 (2008) 7161–7168.
[21] R. Thapa, D. Rhonehouse, D. Nguyen, K. Wiersma, C. Smith, J. Zong, A. Chavez-Pirson, Mid-IR supercontinuum generation in ultra-low loss, dispersion-zero shifted tellurite glass fiber with extended coverage beyond 4.5 μm, Proc. SPIE 8898 (2013), 889808.
[22] S. Kedenburg, C. Strutynski, B. Kibler, P. Froidevaux, F. Désévédavy, G. Gadret, J.-C. Jules, T. Steinle, F. Mörz, A. Steinmann, H. Giessen, F. Smektala, High repetition rate mid-infrared supercontinuum generation from 1.3 to 5.3 μm in robust step-index tellurite fibers, J. Opt. Soc. Am. B 34 (2017) 601–607.
[23] G. Qin, M. Liao, T. Suzuki, A. Mori, Y. Ohishi, Widely tunable ring-cavity tellurite fiber Raman laser, Opt. Lett. 33 (2008) 2014–2016.
[24] G. Qin, A. Mori, Y. Ohishi, Brillouin lasing in a single-mode tellurite fiber, Opt. Lett. 32 (2007) 2179–2181.
[25] M. Deroh, B. Kibler, A. Lemière, F. Désévédavy, F. Smektala, H. Maillotte, T. Sylvestre, J.-C. Beugnot, 2-μm Brillouin laser based on infrared nonlinear glass fibers, Appl. Opt. 58 (2019) 6365–6369.
[26] X. Luo, T.H. Tuan, T.S. Saini, H.P.T. Nguyen, T. Suzuki, Y. Ohishi, Brillouin comb generation in a ring cavity with tellurite single mode fiber, Opt Commun. 426 (2018) 54–57.
[27] T.H. Tuan, L. Zhang, T. Suzuki, Y. Ohishi, Wavelength conversion performance in a tellurite step-index optical fiber, Opt Commun. 381 (2016) 282–285.
[28] G. Ghosh, Sellmeier coefficients and chromatic dispersions for some tellurite glasses, J. Am. Ceram. Soc. 78 (1995) 2828–2830.
[29] S. Kedenburg, T. Steinle, F. Mörz, A. Steinmann, D. Nguyen, D. Rhonehouse, J. Zong, A. Chavez-Pirson, H. Giessen, Solitonic supercontinuum of femtosecond mid-IR pulses in W-type index tellurite fibers with two zero dispersion wavelengths, APL Photon 1 (2016), 086101.
[30] T. Cheng, F. Zhang, S. Li, X. Yan, F. Wang, X. Zhang, T. Suzuki, Y. Ohishi, Experimental investigation of polarization modulation instability in a double-clad single-mode tellurite optical fiber, Appl. Phys. B 126 (2020) 180.
[31] C. Strutynski, P. Froidevaux, F. Désévédavy, J.-C. Jules, G. Gadret, A. Bendahmane, K. Tarnowski, B. Kibler, F. Smektala, Tailoring supercontinuum generation beyond 2 μm in step-index tellurite fibers, Opt. Lett. 42 (2017) 247–250.
[32] P. Froidevaux, A. Lemière, B. Kibler, F. Désévédavy, P. Mathey, G. Gadret, J.-C. Jules, K. Nagasaka, T. Suzuki, Y. Ohishi, F. Smektala, Dispersion-engineered step-index tellurite fibers for mid-infrared coherent supercontinuum generation from 1.5 to 4.5 μm with sub-nanojoule femtosecond pump pulses, Appl. Sci. 8 (2018) 1875.
[33] C. Strutynski, J. Picot-Clémente, A. Lemiere, P. Froidevaux, F. Désévédavy, G. Gadret, J.-C. Jules, B. Kibler, F. Smektala, Fabrication and characterization of step-index tellurite fibers with varying numerical aperture for near- and mid-infrared nonlinear optics, J. Opt. Soc. Am. B 33 (2016) D12–D18.
[34] I. Savelii, F. Desevedavy, J.-C. Jules, G. Gadret, J. Fatome, B. Kibler, H. Kawashima, Y. Ohishi, F. Smektala, Management of OH absorption in tellurite optical fibers and related supercontinuum generation, Opt. Mater. 35 (2013) 1595–1599.
[35] A. Maldonado, M. Evrard, E. Serrano, A. Crochetet, F. Désévédavy, J. Jules, G. Gadret, C. Brachais, C. Strutynski, Y. Ledemi, Y. Messaddeq, F. Smektala, TeO2-ZnO-La2O3 tellurite glass system investigation for mid-infrared robust optical fibers manufacturing, J. Alloys Compd. 867 (2021), 159042.
[36] M. Evrard, T. Combes, A. Maldonado, F. Désévédavy, G. Gadret, C. Strutynski, J. C. Jules, C.H. Brachais, F. Smektala, TeO2-ZnO-La2O3 tellurite glass purification for mid-infrared optical fibers manufacturing, Opt. Mater. Express 12 (2022) 136–152.
[37] I.H. Malitson, Interspecimen comparison of the refractive index of fused silica, J. Opt. Soc. Am. 55 (1965) 1205–1209.
[38] R. El-Mallawany, M.A. Ribeiro, L.S. Lara, E.K. Lenzi, I.A.A. Alsadig, A. Novatski, Refractive index behavior of tellurite glasses, Opt. Mater. 112 (2021), 110810.
[39] T. Boilard, R. Vallée, M. Bernier, Probing the dispersive properties of optical fibers with an array of femtosecond-written fiber Bragg gratings, Sci. Rep. 12 (2022) 4350.
[40] P. Ciacka, A. Rampur, A. Heidt, T. Feurer, M. Klimczak, Dispersion measurement of ultra-high numerical aperture fibers covering thulium, holmium, and erbium emission wavelengths, J. Opt. Soc. Am. B 35 (2018) 1301–1307.
[41] A. Parriaux, K. Hammani, G. Millot, Two-micron all-fibered dual-comb spectrometer based on electro-optic modulators and wavelength conversion, Commun. Phys. 1 (2018) 17.